Extending single-photon optimized superconducting transition edge sensors beyond the single-photon counting regime

Thomas Gerrits,[1,*] Brice Calkins,[1] Nathan Tomlin,[1] Adriana E. Lita,[1] Alan Migdall,[2,3] Richard Mirin,[1] and Sae Woo Nam[1]

[1]National Institute of Standards and Technology, Boulder, CO, 80305, USA
[2]National Institute of Standards and Technology, Gaithersburg, MD, 20899, USA
[3]Joint Quantum Institute, Univ. of Maryland, College Park, MD 20742, USA

*thomas.gerrits@nist.gov

Abstract: Typically, transition edge sensors resolve photon number of up to 10 or 20 photons, depending on the wavelength and TES design. We extend that dynamic range up to 1000 photons, while maintaining sub-shot noise detection process uncertainty of the number of detected photons and beyond that show a monotonic response up to $\approx 6 \cdot 10^6$ photons in a single light pulse. This mode of operation, which heats the sensor far beyond its transition edge into the normal conductive regime, offers a technique for connecting single-photon-counting measurements to radiant-power measurements at picowatt levels. Connecting these two usually incompatible operating regimes in a single detector offers significant potential for directly tying photon counting measurements to conventional cryogenic radiometric standards. In addition, our measurements highlight the advantages of a photon-number state source over a coherent pulse source as a tool for characterizing such a detector.

OCIS codes: (040.5570) Quantum Detectors; (040.3780) Low light level; (120.5630) Radiometry.

References and links

1. G. Eppeldauer and J. E. Hardis, "Fourteen-decade photocurrent measurements with large-area silicon photodiodes at room temperature," Appl. Opt. **30**, 3091–3099 (1991).
2. J. Mountford, G. Porrovecchio, M. Smid, and R. Smid, "Development of a switched integrator amplifier for high-accuracy optical measurements," Appl. Opt. **47**, 5821–5828 (2008).
3. R. J. McIntyre, "Theory of microplasma instability in silicon," J. Appl. Phys. **32**, 983–995 (1961).
4. H. Takesue, S. W. Nam, Q. Zhang, R. H. Hadfield, T. Honjo, K. Tamaki, and Y. Yamamoto, "Quantum key distribution over a 40-db channel loss using superconducting single-photon detectors," Nat. Photonics **1**, 343–348 (2007).
5. T. Gerrits, S. Glancy, T. S. Clement, B. Calkins, A. E. Lita, A. J. Miller, A. L. Migdall, S. W. Nam, R. P. Mirin, and E. Knill, "Generation of optical coherent-state superpositions by number-resolved photon subtraction from the squeezed vacuum," Phys. Rev. A **82**, 031802 (2010).
6. E. Reiger, S. Dorenbos, V. Zwiller, A. Korneev, G. Chulkova, I. Milostnaya, O. Minaeva, G. Gol'tsman, J. Kitaygorsky, D. Pan, W. Sysz, A. Jukna, and R. Sobolewski, "Spectroscopy with nanostructured superconducting single photon detectors," IEEE J. Sel. Topics Quantum Electron. Journal of **13**, 934 –943 (2007).

7. N. Namekata, S. Adachi, and S. Inoue, "1.5 GHz single-photon detection at telecommunication wavelengths using sinusoidally gated ingaas/inp avalanche photodiode," Opt. Express **17**, 6275–6282 (2009).

8. M. A. Krainak, G. Yanga, W. Lu, and X. Sun,"Photon-counting detectors for space-based applications" Detectors and Imaging Devices: Infrared, Focal Plane, SPIE Proc. **7780**, 77801J (2010).

9. P. Walther, J. W. Pan, M. Aspelmeyer, R. Ursin, S. Gasparoni, and A. Zeilinger, "De Broglie wavelength of a non-local four-photon state," Nature **429**, 158–161 (2004).

10. M. W. Mitchell, J. S. Lundeen, and A. M. Steinberg, "Super-resolving phase measurements with a multiphoton entangled state," Nature **429**, 161–164 (2004).

11. K. Tsujino, D. Fukuda, G. Fujii, S. Inoue, M. Fujiwara, M. Takeoka, and M. Sasaki, "Sub-shot-noise-limit discrimination of on-off keyed coherent signals via a quantum receiver with a superconducting transition edge sensor," Opt. Express **18**, 8107–8114 (2010).

12. A. Garg, and N.D. Mermin, "Detector inefficiencies in the Einstein-Podolsky-Rosen experiment," Phys. Rev. D **35**, 3831–3835 (1987).

13. A. R. Beaumont, J. Y. Cheung, C. J. Chunnilall, J. Ireland, and M. G. White, "Providing reference standards and metrology for the few photon-photon counting community," Nucl. Instrum. Meth. A **610**, 183–187 (2009).

14. G. Brida, M. Chekhova, M. Genovese, M. L. Rastello, I. Ruo-Berchera, "Absolute calibration of analog detectors using stimulated parametric down conversion," J. Mod. Optic. **56**, 401–404 (2009).

15. J. A. Chervenak, E. N. Grossman, C. D. Reintsema, K. D. Irwin, S. H. Moseley, and C. A. Allen, "Sub-picowatt precision radiometry using superconducting transition edge sensor bolometers," IEEE Trans. Appl. Supercond., **11**, 593–596 (2001).

16. S. I. Woods, S. M. Carr, A. C. Carter, T. M. Jung, and R. U. Datla, "Calibration of ultra-low infrared power at NIST," SPIE Proc. **7742**, 77421P (2010).

17. R. Klein, R. Thornagel, and G. Ulm, "From single photons to milliwatt radiant power-electron storage rings as radiation sources with a high dynamic range," Metrologia **47**, R33–R40 (2010).

18. G. P. Eppeldauer, and D. C. Lynch, "Opto-mechanical and electronic mesign of a tunnel-trap Si radiometer," J. Res. Natl. Inst. Stan. **105**, 813–828 (2000).

19. J. Y. Cheung, C. J. Chunnilall, G. Porrovecchio, M. Smid, and E. Theocharous, "Low optical power reference detector implemented in the validation of two independent techniques for calibrating photon-counting detectors," Opt. Express **19**, 20347–20363 (2011).

20. A. R. Dixon, Z. L. Yuan, J. F. Dynes, A. W. Sharpe, and A. J. Shields, "Gigahertz decoy quantum key distribution with 1 Mbit/s secure key rate," Opt. Express **16**, 18790–18979 (2008).

21. D. Fukuda, G. Fujii, T. Numata, K. Amemiya, A. Yoshizawa, H. Tsuchida, H. Fujino, H. Ishii, T. Itatani, S. Inoue, and T. Zama, "Titanium-based transition-edge photon number resolving detector with 98% detection efficiency with index-matched small-gap fiber coupling," Opt. Express **19**, 870–875 (2011).

22. R. H. Hadfield, "Single-photon detectors for optical quantum information applications," Nat. Photonics **3**, 696–705 (2009).

23. M. D. Eisaman, J. Fan, A. Migdall, and S. V. Polyakov, "Invited review article: Single-photon sources and detectors," Rev. Sci. Instrum. **82**, 071101 (2011).

24. P. Buzhan, B. Dolgoshein, A. Ilyin, V. Kaplin, S. Klemin, R. Mirzoyan, E. Popova, and M.Teshima, "The cross-talk problem in sipms and their use as light sensors for imaging atmospheric cherenkov telescopes,"Nucl. Instrum. Meth. A **610**, 131–134 (2009).

25. A. J. Miller, S. W. Nam, J. M. Martinis, and A. V. Sergienko, "Demonstration of a low-noise near-infrared photon counter with multiphoton discrimination," Appl. Phys. Lett. **83**, 791–793 (2003).

26. A. E. Lita, A. J. Miller, and S. W. Nam, "Counting near-infrared single-photons with 95% efficiency," Opt. Express **16**, 3032–3040 (2008).

27. B. Cabrera, R. M. Clarke, P. Colling, A. J. Miller, S. Nam, and R. W. Romani, "Detection of single infrared, optical, and ultraviolet photons using superconducting transition edge sensors," Appl. Phys. Lett. **73**, 735–737 (1998).

28. A. G. Kozorezov, J. K. Wigmore, D. Martin, P. Verhoeve, and A. Peacock, "Electron energy down-conversion in thin superconducting films," Phys. Rev. B **75**, 094513 (2007).

29. A. Lamas-Linares, T. Gerrits, N. A. Tomlin, A. Lita, B. Calkins, J. Beyer, R. Mirin, and S. W. Nam, "Transition edge sensors with low timing jitter at 1550 nm," CLEO conference 2012 http://www.opticsinfobase.org/abstract.cfm?URI=QELS-2012-QTu3E.1

30. A. J. Miller, A. E. Lita, B. Calkins, I. Vayshenker, S. M. Gruber, and S. W. Nam, "Compact cryogenic self-aligning fiber-to-detector coupling with losses below one percent," Opt. Express **19**, 9102–9110 (2011).

31. P. R. Tapster, S. F. Seward, and J. G. Rarity, "Sub-shot-noise measurement of modulated absorption using parametric down-conversion," Phys. Rev. A **44**, 3266–3269 (1991).

32. G. Brida, L. Ciavarella, I. P. Degiovanni, M. Genovese, A. Migdall, M. G. Mingolla, M. G. A. Paris, F. Piacentini, and S. V. Polyakov, "Ancilla-assisted calibration of a measuring apparatus", Phys. Rev. Lett., **108**, 253601 (2012).

33. K. D. Irwin, and G. C. Hilton, "Transition-edge sensors," Cryogenic Particle Detection, Top. Appl. Phys. **99**, 63–152 (2005).

34. K. D. Irwin, "An application of electrothermal feedback for high resolution cryogenic particle detection," Appl.

Phys. Lett. **66**, 1998–2000 (1995).

35. E. Figueroa-Feliciano, B. Cabrera, A. Miller, S. Powell, T. Saab, and A. Walker, "Optimal filter analysis of energy-dependent pulse shapes and its application to TES detectors," Nucl. Instrum. Meth. A **444**, 453–456 (2000).

36. D. Fixsen, S. Moseley, B. Cabrera, and E. Figueroa-Feliciano, "Pulse estimation in nonlinear detectors with nonstationary noise," Nucl. Instrum. Meth. A **520**, 555–558 (2004).

37. Z. H. Levine, T. Gerrits, A. L. Migdall, D. V. Samarov, B. Calkins, A. E. Lita, and S. W. Nam, "An algorithm for finding clusters with a known distribution and its application to photon-number resolution using a superconducting transition-edge sensor," J. Opt. Soc. Am. B **29**, 2066–2073 (2012).

38. T. Gerrits, M. J. Stevens, B. Baek, B. Calkins, A. Lita, S. Glancy, E. Knill, S. W. Nam, R. P. Mirin, R. H. Hadfield, R. S. Bennink, W. P. Grice, S. Dorenbos, T. Zijlstra, T. Klapwijk, and V. Zwiller, "Generation of degenerate, factorizable, pulsed squeezed light at telecom wavelengths," Opt. Express **19**, 24434–24447 (2011).

1. Introduction

Detection of light is an important enabling technology for many applications. Present detection capabilities are already impressive. As just one example, room temperature devices, such as silicon photodiodes can have high detection efficiencies and low noise, which allows for detection of light over a dynamic range from milliwatts to picowatts (or even lower) when operated in analog-mode [1, 2], and even to attowatt levels when operated in single-photon counting avalanche-mode [3]. This large dynamic range presents challenges in how to accurately calibrate such a device; and in recent years, the advances in detection technology and the demands of applications at lower detection levels are only increasing the challenge. Examples of applications driving advances in single-photon-counting technologies include quantum information applications [4, 5], spectroscopy [6], certain telecommunication applications [7], space based applications [8], a number of metrology applications [9–11], and even efforts focused on fundamental physical questions [12–14].

Metrology efforts dealing with measurements over such a large dynamic range have taken two directions, either a) pushing existing "classical" high optical-power level radiometric measurements to devices that can maintain high accuracy at low light levels, or b) pushing the capabilities of single-photon measurements to higher photon rates. Examples of the former include the development of cryogenic radiometers for optical powers much below the typical ≈ 0.1 mW design levels of these radiometric standards [15, 16], the development of techniques to extend and characterize the linearity of existing standards like the synchrotron to very low light levels [17], and the development of high dynamic range trap detector amplifier packages [18, 19]. The latter direction includes efforts to improve the capabilities of single-photon technology with a particular focus on increasing the maximum rates at which photons can be counted. One example of how maximum counts can be improved is through careful gating of the detector so that afterpulsing and deadtimes are minimized [20], and now detectors that can be gated at 100 MHz or higher are available.

Along the lines of both of these goals, we present here the results of our efforts to explore and extend the capabilities of the transition-edge sensor (TES), an already very remarkable detector. To date this device has demonstrated photon-counting efficiencies near 100% and extremely well resolved photon-number peaks to ≈ 10 photons at 800 nm [21]. We take a TES optimized for photon counting and show that the detector allows photon-number to be extracted beyond the shot noise limit (albeit not with single-photon resolution) for up to ≈ 1000 photons. This is well beyond the 10 to 20 photons typically reported for TESs, and we further show that the device retains some sensitivity beyond 10^6 photons per pulse (or 10^9 photons/s in our case). This latter characteristic may be particularly advantageous as a radiometric tool for bridging the gap from single-photon sensitivity to picowatt-levels that analog detectors can detect.

The TES is a recent development in a long history of optical photon counting which began almost a century ago with photo-multiplier tubes (PMTs), which have been and continue to

be a workhorse for many single-photon optical detection applications. The PMT was joined in the 1960s by silicon avalanche photodiodes (Si APDs) offering solid state operation among other advantages. These Si APDs generally operate near room temperature, and because of the high purity of the silicon avalanche region, they can achieve high detection efficiencies with low dark count rates of less than 100 Hz [22, 23]. Recently, about one hundred photons were resolved by use of a multi-pixel silicon photon counter [24]. New devices that have expanded the spectral range of photon counting to telecom wavelengths around 1550 nm include InGaAs avalanche photodiodes (InGaAs APDs) and superconducting nanowire single-photon detectors (SNSPDs) [22, 23]. The InGaAs APDs however, exhibit high dark count probabilities and as a result must be operated in gated-bias mode so that the detector is only active during a short time window when a photon is expected. The SNSPDs operate at cryogenic temperatures ($\approx$ 4 K or lower) and can show very small timing jitter of less than 30 ps and usually have less than 1 kHz dark count rates [22, 23]. The TES, also a superconducting detector operates as a microcalorimeter and measures the amount of heat absorbed in the detection region. Therefore, for monochromatic light, the TES is intrinsically photon-number resolving, and can distinguish peaks due to more than 15 photons at 1550 nm [25]. Also, due to the low thermal noise of the sensor and the read-out circuit at sub-Kelvin temperatures, TESs show no dark counts. Furthermore, by embedding the detector in a stack of appropriate dielectric materials, the TES can detect all photons with near-unity efficiency [26]. The temporal response of these devices however, is determined by thermal relaxation mechanisms, and is therefore limited to $\approx$ 100 ns timescales [27, 28], although faster response times are in the offing [29]. The ultimate photon-number resolution of a TES is determined by its thermal characteristics and the steepness of the superconducting-to-resistive transition. While heating the TES beyond its transition region will place the detector in its normal conductance regime and degrade its single-photon-resolving sensitivity, some sensitivity still remains. Exploration of how far the capabilities of the TES can be pushed into that region is the motivation for our efforts here.

Before getting into our measurements we lay the groundwork by discussing issues limiting detector calibrations and presenting a model of the TES operation.

2. Calibration of Single-Photon Detectors

Calibration of single-photon detectors is typically achieved by attenuating a coherent laser source, determining the mean photon number ($\bar{N}$) in some measurement time and comparing it to the output of the photon-counting detector when illuminated by that attenuated source [30]. The uncertainties associated by this scheme, however, are inherently limited by the shot noise of the photon source (σ_{Coh}), in this case a coherent laser beam, which obeys Poisson statistics and scales as $\sqrt{\bar{N}}$. Moreover, technical and other noises of the photon source often increase the uncertainty beyond the inherent shot noise of the source. Therefore, to determine the noise of the detector, the noise of the source must be backed out first. Thus, in a detector calibration the source noise can severely limit the ultimate accuracy. As we shall see, this becomes more of a problem when measuring the noise of high-efficiency photon-number-resolving detectors such as the TES. One solution to this problem is to replace the noisy laser photon source with a source of heralded photon-number states, *i.e.* Fock states, as Fock states are not subject to shot or other noises. A measurement of a detector made with Fock state illumination would have only the shot noise uncertainty associated with the detection efficiency of the device (and, of course, any other uncertainties associated with the detector itself). The spread of the photon number distribution for an N_{F}-Fock state is limited only by the detection inefficiency and is given by the variation of the binomial distribution:

$$\sigma_{\mathrm{F}}(\eta) = \sqrt{N_{\mathrm{F}}\eta(1-\eta)}, \tag{1}$$

where η is the overall detection efficiency and N_F is the number of photons present in the Fock state. (Related examples of employing nonclassical states produced via parametric downconversion for sub-shot noise measurement of transmittance have been implemented [31], as has a quantum characterization of a detector's positive-operator valued measure (POVM) [32].)

3. Modeling transition edge sensor response

Typically, it is sufficient to use a two-body thermal model to describe the temperature evolution of the electrons and phonons in the TES. Furthermore, for low light levels the equations are often linearized. However, under bright pulse illumination it is necessary to use a three-body model that is not linearized to represent the thermal evolution of the TES [33]:

$$
\begin{aligned}
C_e(T_e)\frac{dT_e}{dt} &= -\kappa_{e-p}(T_e^5 - T_p^5) + P_J + \eta_\gamma \delta(t)P_\gamma \\
C_p(T_p)\frac{dT_p}{dt} &= -\kappa_{p-b}(T_p^4 - T_b^4) + \kappa_{e-p}(T_e^5 - T_p^5) + (1 - \eta_\gamma)\delta(t)P_\gamma,
\end{aligned}
\tag{2}
$$

where $C_e(T_e)$ and $C_p(T_p)$ are the temperature-dependent heat capacities of the electron and phonon systems. T_e, T_p, and T_b are the electron, phonon and thermal bath temperatures, respectively and $\delta(t)$ is the Dirac delta function. κ_{e-p} and κ_{p-b} are the thermal coupling parameters for the electron-phonon and phonon-bath thermal links. P_J is the joule heating power due to the TES voltage bias: $P_J = V_b^2/R(T)$, where V_b is the bias voltage and $R(T)$ is the temperature-dependent TES resistance [34]. $\delta(t)P_\gamma$ is the absorbed optical power incident at the TES at initial time $t = 0$, and η_γ is the fraction of the optical energy remaining in the electron system after the optical pulse is absorbed and $1 - \eta_\gamma$ is the fraction of the optical energy lost to the phonon system. We assume the light's absorption and the subsequent energy loss to the phonon system happens instantaneously. Therefore, the initial electron temperature, $T_e(0)$, can be calculated by the amount of photon energy absorbed by the sensor $E_p = \eta \bar{N}\hbar\omega = \bar{N}_a\hbar\omega = \int \delta(t_0)P_\gamma dt$ and the portion of that energy absorbed and retained by the electron system:

$$
\eta_\gamma E_p = \int_{T_c}^{T_e(0)} C_e dT = \int_{T_c}^{T_e(0)} \mathscr{C}_e \cdot V \cdot T \, dT,
\tag{3}
$$

where $\bar{N}_a$ is the absorbed mean photon number per pulse, $\mathscr{C}_e \cdot T$ is the volumetric electronic heat capacity, V is the sensor volume and T_c is the sensor's critical temperature. Similarly we can calculate the initial heat-up of the phonon system:

$$
(1 - \eta_\gamma)E_p = \int_{T_b}^{T_p(0)} C_p dT = \int_{T_b}^{T_p(0)} \mathscr{C}_p \cdot V \cdot T^3 \, dT,
\tag{4}
$$

where $\mathscr{C}_p \cdot T^3$ is the volumetric phonon heat capacity. Note that because of the large range of temperatures involved, we have to take into account the temperature dependencies of the heat capacities.

4. Experimental setup

For our study we used a TES consisting of a 25 μm $\times$25 μm$\times$20 nm tungsten film with a superconducting transition temperature of 140 mK. The TES was embedded in a stack of dielectrics and had an overall detection efficiency of 89 ± 1.5 % at 1550 nm [30]. The complete sensor was fabricated on a 325 μm thick silicon substrate. We mounted the TES inside a commercial

adiabatic demagnetization refrigerator (ADR) and used a commercial telecom fiber to couple the light pulses from the attenuated laser at room temperature to the detector inside the ADR. The cold stage of the ADR was held at a regulated temperature of 90 ± 1 mK. Voltage biasing of the TES ensured that the sensor was biased in the transition region at $T_c \approx 140$ mK before the arrival of each light pulse. We delivered bright light pulses using a pulsed coherent laser source at a wavelength of 1550 nm at a repetition rate of 1 kHz. Determination of the laser pulse energy (in terms of the mean photon number per pulse, $\bar{N}$) was achieved by comparison to a calibrated detector as described in Ref. [30]. The maximum average power inside the TES input fiber was 850 pW, and due to the TES's detection efficiency, the maximum average power absorbed by the TES was 760 pW.
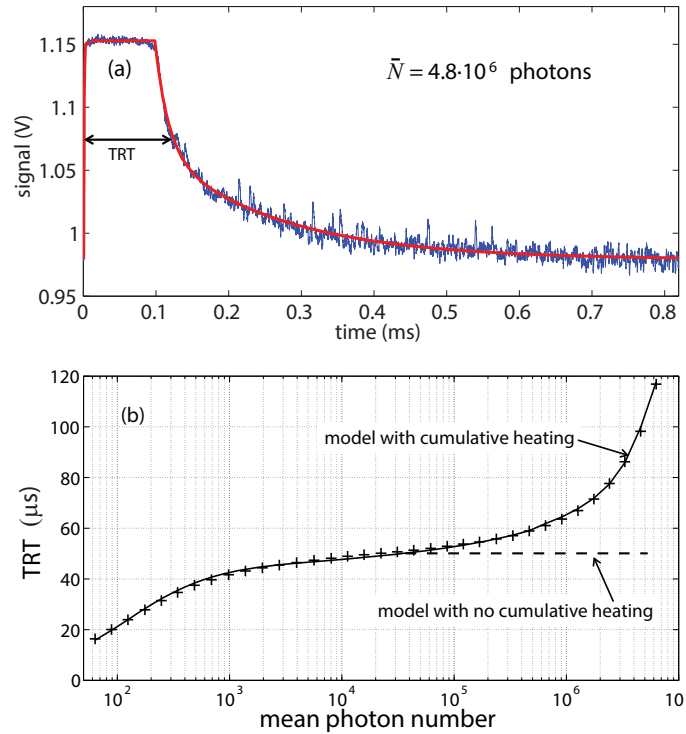

Fig. 1. (a) TES output signal time response (blue line) and fit (red line) after illumination with a coherent laser pulse with $\bar{N} = 4.8 \cdot 10^6$ photons. (b) Thermal relaxation time (TRT) of the TES (crosses), as a function of mean input photon number. The numerical integration of Eq. (2) for each input mean photon number: model with cumulative heating (solid line), model with no cumulative heating (dashed line).

5. Results

The blue curve in Fig. 1(a) shows a typical response of the TES to illumination with a bright laser pulse. In this particular case, the TES was heated to ≈ 21 K after illumination with a pulse of light containing ≈ 4.8 million photons. A few tens of nanoseconds after the bright pulse is absorbed, the output signal shows the TES entering the normal-conductance region where the observed signal remains approximately constant until the TES cools back down to the transition region and the decay response is seen. The thermal relaxation time (TRT) - the time it

takes the TES to cool back down to the transition region - depends on the amount of energy absorbed in the TES. We use this TRT parameter as a measurement proxy for photon number. We determined the TRT by fitting the TES response using a two-part piecewise fitting function to handle separately the rising and falling portions of the response. The first function, capturing the rising edge of the TES response, yields the time when the signal passes a threshold (chosen to be 50% of the maximum signal amplitude). The second function, capturing the trailing edge, yields the time the response passes the 50% threshold on the down-slope. The difference between these two times is the TRT. The red line in Fig. 1(a) shows that this piecewise function can describe our data well. We recorded and fitted 20480 individual traces for each $\bar{N}$. We found that fitting the data to our simple model works well for $\bar{N} > 60$. The crosses in Fig. 1(b) show the mean of the TRTs obtained from the fits as a function of $\bar{N}$. A strong dependence of the TRT with $\bar{N}$ is observed up to $\bar{N} \approx 1000$ photons. The subsequent flatter region is due to the strong initial heating of the electron system when absorbing brighter laser pulses. By examining Eq. (2), and noting that initially the electron temperature is much greater than the phonon temperature, one finds that the T_e^5 term dominates the thermal relaxation dynamics and causes the electron system to couple the energy quickly into the phonon system. Therefore, at high laser pulse energies the change in the total TRT with respect to $\bar{N}$ is smaller than for low laser pulse energies. This can also be found by numerically integrating Eq. (2), shown by the solid line in Fig. 1(b). The simulation fits our data well and yields the following parameters: $\kappa_{e-p} = 9.3$ nWK^{-5}; $\kappa_{p-b} = 150$ nWK^{-4}; $\mathscr{C}_e = 123$ Jm^{-3}K^{-2}; $\mathscr{C}_p = 4.0$ Jm^{-3}K^{-4}; $\eta_\gamma = 0.61$. The upturn of the TRT dependence at very high input mean photon numbers ($\bar{N} > 10^5$) is due to heating of the TES substrate (heat bath). Due to the relatively short delay between successive laser pulses (1 ms), the substrate experiences cumulative heating. This heating also ultimately limits the maximum number of photons that can be detected at a given laser repetition rate. This limit is reached when the substrate temperature is close to or in excess of the TES's transition temperature of 140 mK. The dashed line shows the predicted sensor response when no cumulative substrate heating is present. It remains flat beyond 10000 photons.

Figure 2(a) shows a summary of the measurement uncertainties in units of photon number as a function of $\bar{N}$. These are the uncertainties of the measurement of the energy proxy $\mathscr{E}_P$, which in this case is the TRT as just described, or the matched filter result as described below. Included in the figure are the overall uncertainties, the uncertainties due to the detection process and the uncertainties due to the shot noise of the input photon state. We calculated standard deviations in units of photon number ($\sigma_{\bar{N}}$) via:

$$\sigma_{\bar{N}} = \left[\frac{\partial \bar{\mathscr{E}}_P}{\partial \bar{N}} \right]^{-1} \cdot \sigma_{\mathscr{E}_P}, \qquad (5)$$

where $\bar{\mathscr{E}}_P$ and $\sigma_{\mathscr{E}_P}$ are the mean and the standard deviation of the measured outcomes for each $\bar{N}$, respectively. In the appendix we show that we can estimate an upper bound for the uncertainty of the detection process by subtracting the input state shot noise from the variance of the measured outcomes: $\sigma_d^2 \leq \sigma_{\bar{N}}^2 - \bar{N}$. We define the photon number uncertainty of a single detection as $\sqrt{\sigma_d^2}$. This uncertainty contains the read-out and detector noise. The uncertainty resulting from the input state shot noise after being absorbed by the TES scales as $\sqrt{\bar{N}_a}$ (dashed blue line). The upper-bound estimates of the uncertainty due to the detection process (black squares) show measurements limited by the source shot noise for $\bar{N} < 1000$. For $\bar{N} > 1000$, the detection process uncertainty becomes larger than the shot noise due to the source and increases dramatically for $\bar{N} > 10000$. The reason for this upturn is the small change of TRT with respect to the absorbed number of photons. This value is about 5000 times smaller than in the region for $\bar{N} < 1000$. The theoretical variation of the TRT based on the confidence of the fit (black
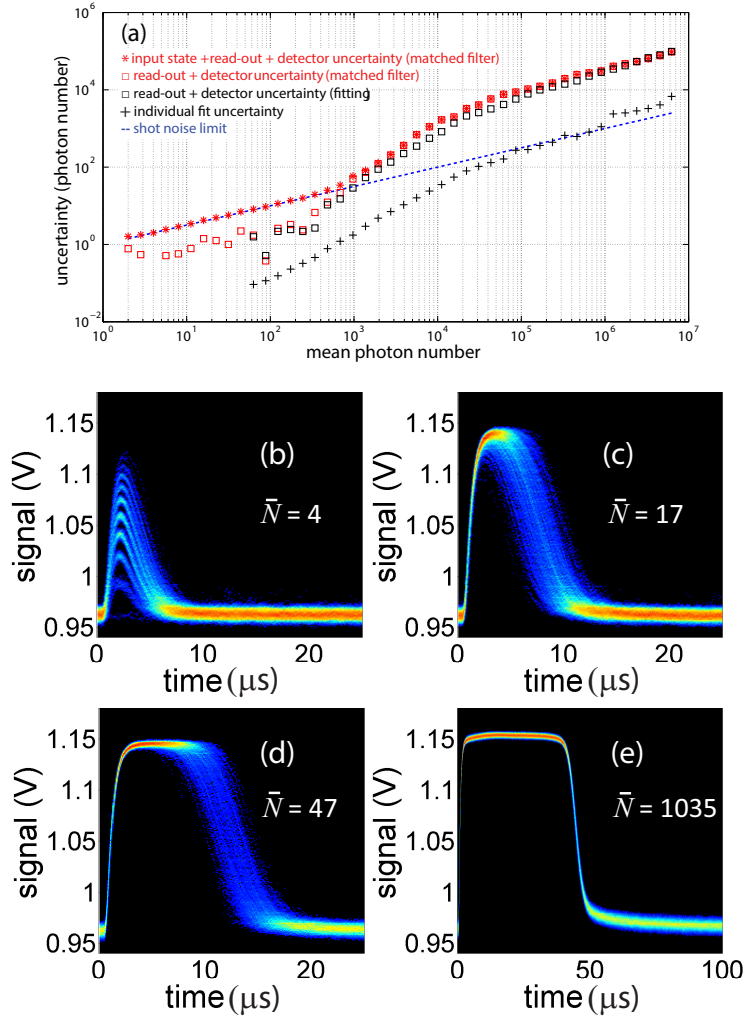
Fig. 2. (a) Standard deviations of photon-number determinations as a function of input mean photon number. Total measured uncertainty, as determined by the matched filter analysis (red stars). Uncertainty associated with detection process, *i.e.* read-out plus detector, as determined by the matched filter analysis (red squares) or the fitting routine (black squares). Fit uncertainty representing a 1σ confidence interval determined from each fit to an individual response (black crosses). Input state shot noise (blue dashed line). (b)-(e). Families of raw response curves for four different input mean photon numbers $\bar{N}$ as labeled.

crosses) was obtained from a 1σ confidence interval on all fitting parameters and by standard error propagation. This variation is caused by the noise in the electrical read-out and gives a lower bound on the detection process uncertainty, because this is an uncertainty of a single fit to a single TES response. Thus, it does not contain any shot-to-shot variation, *e.g.* electron-phonon interaction statistics or variation of our laser source.

In addition to the fitting procedure described above, we also analyzed the data by use of a matched filter [35, 36]. This matched filter method relies on the creation of a template that is the average of all individual TES response curves, *i.e.* the ideal curve shape without noise. The inner product of the template with each individual response curve yields a proxy for the energy that has been absorbed by the sensor with high signal-to-noise ratio. However, we note that this method is not optimal in the normal conductance regime. Optimal performance using this method can be achieved in the limit of white noise and when the overall pulse shape does not change with photon number input [35, 36]. The standard deviation of 20480 individual photon number determinations for each input $\bar{N}$ is shown in Fig. 2(a) (red stars), along with the upper bound estimate of the detection process uncertainty after subtracting the input state shot noise (red squares).

Figures 2(b)-2(e) show 1024 raw TES response curves for different $\bar{N}$. Figure 2(b) shows typical TES response curves for $\bar{N} = 4$. The photon-number-resolving capability in the low photon number regime is demonstrated here. Figure 2(c) shows the output response for $\bar{N} = 17$. In this regime the TES is at the upper edge of its transition region and starts to enter the normal conductance regime. Partial photon-number resolution can still be observed. An extensive analysis of an algorithm aimed at improved extraction of photon number information from a large set of TES responses to coherent pulses with some mean photon number is reported in Ref. [37]. In that case, it was possible to see photon number peaks up to 23. Figure 2(d) shows the TES responses for $\bar{N} = 47$. Figure 2(e) shows the TES responses after illumination with $\bar{N} = 1035$. At this point the TES photon number determination is limited by detection noise, rather than being limited by the shot noise of the source.

6. Calibration with photon number states

The above results were obtained using a coherent state laser source. However, such a source with its Poisson statistics and possible additional other noises, can only yield an upper bound on the detection uncertainty. A Fock state source, on the other hand, with its well defined photon number, would allow for lower total measurement uncertainties to be achieved. Figure 3(a) shows a simulation of the photon number statistics, as would be seen by a TES with a detection efficiency of 89 %, for Fock states with $N_F = 1, 20$, and 80 (red bars), and for comparison coherent states with $\bar{N} = 1, 20$, and 80 (black bars). Clearly, the variation in the photon-number measurement is higher for the coherent state inputs with their spread of photon numbers, than for Fock state inputs, where the variation is only due to the nonunity detection efficiency (see Eq. (1)). Figure 3(b) shows an actual measurement of a heralded single-photon Fock state from a down-conversion source [38] (red bars). The heralded measurement shows a fidelity of 47 % to a single photon state (which would have a probability of one for a photon number of one, and all other photon numbers would have probability zero). The fidelity's deviation from unity is mainly due to the inefficient coupling of the down-converted light into our telecom fiber. However, visible is the decreased variance in photon number distribution when comparing it to the simulation of a coherent state with a mean photon number of 0.58 (black bars), *i.e.* equal to the mean photon number of the heralded state.
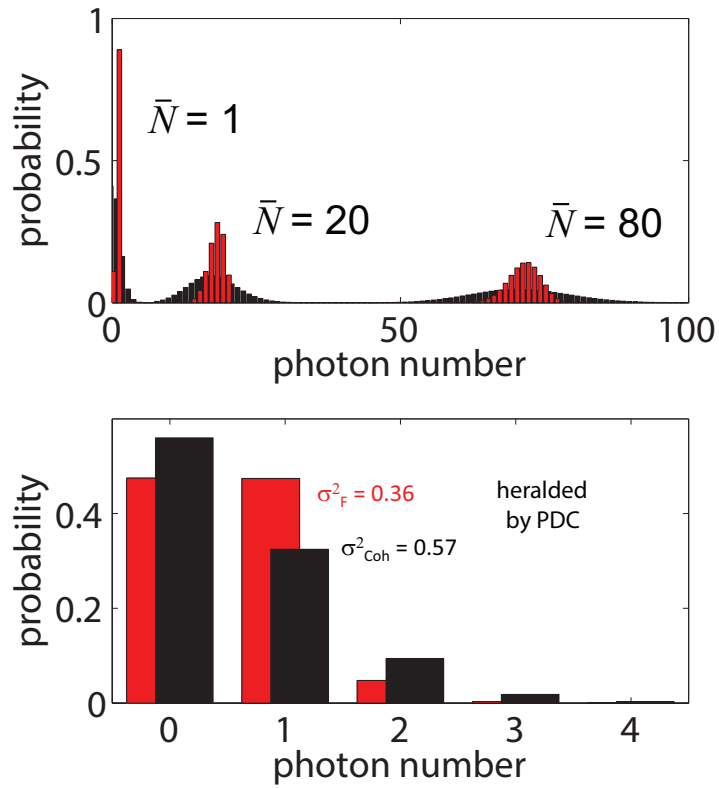
Fig. 3. (a) Simulation of photon-number statistics for different input states. The red bars show the anticipated TES photon number response when illuminating the TES with an $N_F = 1$, 20, and 80 Fock states. The black bars show the TES response when illuminating with a coherent state with $\bar{N} = 1$, 20, and 80. (b) Data for a heralded photon state from parametric down-conversion (PDC).

7. Conclusion

In conclusion, we have demonstrated the operation of a photon-number-resolving transition edge sensor beyond the single-photon counting regime up to $5.6 \cdot 10^6$ absorbed photons in a single pulse, and at the operational repetition rate of 1 kHz the TES records $5.6 \cdot 10^9$ photons per second, corresponding to an absorbed average power of 760 pW. Our results show that the intrinsic energy resolution and single-photon sensitivity of the TES provides a route towards mating bright light level (picowatts) photo detection with single-photon counting. In principle, the TES allows for nanowatt light level detection starting in the single photon regime. The detection process uncertainty was found to be below the input state shot noise up to $\bar{N} = 1000$ for single shot measurements. Better determination of the overall variation in the measurement outcome can be achieved by use of photon number (Fock) states, offering strong impetus for their development.

Appendix

In this appendix, we show that by subtracting the input-state shot noise from the variation in the measurement outcome, we gain an upper bound on the uncertainty associated with a single detection. The overall energy distribution of an ensemble of detections is created by the convolution of the input-state Poisson distribution and the variance of the detection process. When we assume an evenly spaced energy-peak distribution with absorbed photon number, *i.e.* linear detector response, we can write exactly:

$$\sigma_{\bar{N}}^2 = (\bar{N} + \sigma_{\rm d}^2), \tag{6}$$

which is the quadrature sum of the input state shot noise ($\sqrt{\bar{N}}$) and the uncertainty of the detection process $\sigma_{\rm d}$.

  In the case of the TES, however, the detector response becomes non-linear above a few photons. Hence Eq. (6) is no longer valid. However, in the following we show that Eq. (6) still yields an upper bound on the detection process uncertainty.

  We can assume a Poisson distribution of the absorbed input state:

$$p_k = \frac{\mu^k}{k!} e^{-\mu}, \tag{7}$$

where p_k is the probability that the photon number is k with a mean of μ. We can model the non-linear TES response by: $\mathscr{E}(k) \propto [k - \Delta(k)]$, where $\Delta(k)$ is the difference between the deviation from a linear detector response. $\mathscr{E}(k)$ is the proxy for the energy measurement. $\Delta(k)$ is a function of k. Also $\mathscr{E}(k) > 0$ and $\mathscr{E}(k) \to k$ for $k \to 0$ and $\mathscr{E}(k) \to C$, for $k \to \infty$, where C is constant. $\mathscr{E}(k)$ is a continuous, monotonically increasing function. Let the measurement outcomes for each photon number k be spread by a Gaussian distribution with standard deviation σ_x:

$$G_k(x) = \frac{1}{\sigma_x \sqrt{2\pi}} \exp\left[-\frac{(x - \mathscr{E}(k))^2}{2\sigma_x^2} \right], \tag{8}$$

where x is a continuous representation of photon number. The total distribution when convolved with the input state shot-noise then becomes:

$$G_\Sigma(x, k) = \frac{1}{\sigma_x \sqrt{2\pi}} \sum_{k=0}^{\infty} \frac{\mu^k}{k!} e^{-\mu} \exp\left[-\frac{(x - \mathscr{E}(k))^2}{2\sigma_x^2} \right]. \tag{9}$$

The variance of this distribution can be calculated via:

$$\sigma_\varepsilon^2 = \int_{-\infty}^{+\infty} \left[x - \bar{\mathscr{E}} \right]^2 G_\Sigma(x,k)dx, \tag{10}$$

where $\bar{\mathscr{E}}$ is the expected value of the TES response x. Using $\int_{-\infty}^{+\infty} x^2 \exp\left[-x^2\right] = \frac{\sqrt{\pi}}{2}$ and integrate over x we find:

$$\sigma_\mathscr{E}^2 = e^{-\mu} \sum_{k=0}^{\infty} \frac{\mu^k}{k!} \left[(\mathscr{E}(k) - \mu)^2 + \sigma_x^2 \right], \tag{11}$$

which is the variance in energy distribution. The expected value of the TES response x is calculated via:

$$\bar{\mathscr{E}} = \sum_{k=0}^{k=\infty} p_k \mathscr{E}(k) = e^{-\mu} \sum_{k=0}^{k=\infty} \frac{\mu^k}{k!} \mathscr{E}(k). \tag{12}$$

To calculate the variance in photon number we apply:

$$\sigma_N^2 = \left| \frac{\partial \bar{\mathscr{E}}}{\partial \mu} \right|^{-2} \cdot \sigma_\mathscr{E}^2 \tag{13}$$

$$\frac{\partial \bar{\mathscr{E}}}{\partial \mu} = e^{-\mu} \sum_{k=0}^{\infty} \frac{\mu^{k-1}}{k!} \mathscr{E}(k) \left[k - \mu \right].$$

Combining Eq. (13) and Eq. (11) yields:

$$\sigma_N^2 = \frac{\sum_{k=0}^{\infty} \frac{\mu^k}{k!} \left[(\mathscr{E}(k) - \mu)^2 + \sigma_x^2 \right]}{e^{-\mu} \left[\sum_{k=0}^{\infty} \frac{\mu^{k-1}}{k!} \mathscr{E}(k) \left[k - \mu \right] \right]^2}. \tag{14}$$

As $\mathscr{E}(k)$ is a monotonically increasing function, we need only to consider the two limits, $\mu \to 0$ ($\mathscr{E}(k) \to k$) and $\mu \to \infty$ ($\mathscr{E}(k) \to C$). For $\mu \to 0$, using $\Sigma_{k=0}^{\infty} k^2 \frac{\mu^k}{k!} = (\mu + \mu^2)e^\mu$, $\Sigma_{k=0}^{\infty} k \frac{\mu^k}{k!} = \mu e^\mu$ and $\Sigma_{k=0}^{\infty} \frac{\mu^k}{k!} = e^\mu$ we get:

$$\lim_{\mu \to 0} \sigma_N^2 = \frac{\sum_{k=0}^{\infty} \frac{\mu^k}{k!} \left[((k-\varepsilon) - \mu)^2 + \sigma_x^2 \right]}{e^{-\mu} \left[\sum_{k=0}^{\infty} \frac{\mu^{k-1}}{k!} (k-\varepsilon) \left[k - \mu \right] \right]^2} \tag{15}$$

$$= \frac{\varepsilon^2 + \mu + \sigma_x^2}{1} > \mu + \sigma_x^2,$$

where $(k - \varepsilon) \to k$ is the first order approximation of $\mathscr{E}(k)$ for $\mu \to 0$, and $\varepsilon^2 > 0$. Equation (15) shows that in the limit of $\mu \to 0$, the σ_N^2 is always larger (by ε^2) than the shot noise caused by the input state and the TES Gaussian spread $\mu + \sigma_x^2$. For $\mu \to \infty$, Eq. (15) reads:

$$\lim_{\mu \to \infty} \sigma_N^2 = \frac{\sum_{k=0}^{\infty} \frac{\mu^k}{k!} \left[(C - \mu)^2 + \sigma_x^2 \right]}{e^{-\mu} \left[\sum_{k=0}^{\infty} \frac{\mu^{k-1}}{k!} C \left[k - \mu \right] \right]^2} \tag{16}$$

$$= \frac{(C - \mu)^2 + \sigma_x^2}{e^{-\mu} \left[\sum_{k=0}^{\infty} \frac{\mu^{k-1}}{k!} C \left[k - \mu \right] \right]^2} \to \infty,$$

as the denominator goes to zero.

Thus, the uncertainty expressed in units of photon number derived from the non-linear TES response is always greater than the quadrature sum of the input state Poisson noise and the Gaussian TES noise. This means that when subtracting the input state shot noise from the variance of the measurement outcomes we expect to calculate an upper limit on the detection noise associated with a single detection.